Variation of the charge dynamics in bandwidth- and filling-controlled metal-insulator transitions of pyrochlore-type molybdates

István Kézsmárki, N. Hanasaki, K. Watanabe, S. Iguchi, Y. Taguchi, S. Miyasaka, Y. Tokura

Angaben zur Veröffentlichung / Publication details:

Kézsmárki, István, N. Hanasaki, K. Watanabe, S. Iguchi, Y. Taguchi, S. Miyasaka, and Y. Tokura. 2006. "Variation of the charge dynamics in bandwidth- and filling-controlled metal-insulator transitions of pyrochlore-type molybdates." *Physical Review B* 73 (12): 125122. https://doi.org/10.1103/physrevb.73.125122.

Variation of the charge dynamics in bandwidth- and filling-controlled metal-insulator transitions of pyrochlore-type molybdates

I. Kézsmárki,[1,2,3] N. Hanasaki,[1] K. Watanabe,[1] S. Iguchi,[1,2] Y. Taguchi,[4] S. Miyasaka,[1] and Y. Tokura[1,2,5]
[1]*Department of Applied Physics, University of Tokyo, Tokyo 113-8656, Japan*
[2]*Spin Superstructure Project, ERATO, Japan Science and Technology Agency (JST), Tsukuba 305-8562, Japan*
[3]*Electron Transport Research Group of the Hungarian Academy of Science and Department of Physics, Budapest University of Technology and Economics, 1111 Budapest, Hungary*
[4]*Institute for Materials Research, Tohoku University, Sendai 980-8577, Japan*
[5]*Correlated Electron Research Center (CERC), National Institute of Advanced Industrial Science and Technology (AIST), Tsukuba 305-8562, Japan*
(Received 5 December 2005; revised manuscript received 26 January 2006; published 30 March 2006)

The systematics of the bandwidth- and filling-controlled metal-insulator transitions (MITs) have been investigated for $R_2Mo_2O_7$ family (R=Nd, Sm, Eu, Gd, Dy, and Ho) by infrared spectroscopy. The substantial role of electron correlation in driving the MIT is verified. With changing the R ionic radius (r) or equivalently the one-electron bandwidth (W), the MIT occurs in a continuous manner at $r_c \approx r(R=\mathrm{Gd})$. The $T=0$ K gap continuously vanishes as $\Delta \propto (r_c - r)$, while at the metallic side the linear decrease of Drude weight is followed toward r_c. In the metallic compounds, some of the infrared-active phonon modes show remarkably large Fano asymmetry correlating with the Drude weight. These Mo-O-Mo bending modes strongly couple to the conduction electrons via effective modulation of the bandwidth. Even for $r \lesssim r_c$ a minimal level of hole doping closes the correlation gap, for example, the barely insulating $Gd_2Mo_2O_7$ is turned to an incoherent metal by 5% partial substitution of Gd^{3+} with Ca^{2+}. However, even on further doping no coherent electronic states are formed, indicating the role of the disorder-induced localization effect besides the dominant correlation effects.

DOI: 10.1103/PhysRevB.73.125122 PACS number(s): 71.30.+h, 71.27.+a, 78.20.−e

I. INTRODUCTION

The class of metal-insulator transitions (MITs) categorized as Mott transition, in which the localization of the charge carriers is governed by correlation effects, has been extensively studied in the past several decades since the idea was first proposed by Mott in 1949.[1] However, the genuine Mott transition, which does not break any global symmetry and has no order parameter other than the local charge compressibility, has been observed only in a few cases. One such rare example is the transition from paramagnetic Mott insulator to paramagnetic metal controlled by the bandwidth as recently reported for the two-dimensional (2D) organic conductor family $\kappa-(\mathrm{BEDT\text{-}TTF})_2X$ with geometrical frustration effect.[2] Most of correlation-driven MI phenomena are accompanied by spin, charge, and/or orbital order. These have been observed in many 3*d*-electron systems, and a coherent picture is being developed[3,4] about the mechanism of the electron localization. However, 4*d*-electron systems with relatively wider bandwidth have only recently become a hot spot of condensed matter physics.[5–7] Among them, Mo oxides with pyrochlore structure, $R_2Mo_2O_7$, can provide a unique arena to address this question, as they undergo a MIT by changing the rare-earth component R.[8–14]

Both magnetic and transport properties of pyrochlore-type molybdates arise from the behavior of the electrons populating the t_{2g} subspace of Mo 4*d*-levels as confirmed by photoemission experiments and band calculations.[15] Recently, Solovyev[16] applied a Hartree-Fock approach, using the results of local-density approximation (LDA) as a starting point and considering both on-site Coulomb and spin-orbit interaction for the Mo 4*d* electrons. The trigonal distortion splits t_{2g} levels to a higher-lying $e(t_{2g})$ doublet and to a lower-lying a_{1g} state. These bands overlap on the level of LDA, but again can be separated by the on-site Coulomb interaction. As even a more remarkable effect, a charge gap opens in $e(t_{2g})$ for $U \gtrsim 2.5$ eV. Consequently, there is a localized electron at the a_{1g} level, while the other electron in the $e(t_{2g})$ states can be either localized or itinerant, depending on the relative strength of the electron correlation. The interaction between the neighboring Mo spins is antiferromagnetic (AF) for a_{1g} and ferromagnetic (FM) for $e(t_{2g})$ electrons, due to superexchange and double exchange mechanism, respectively. According to their balance, the formation of either FM or spin-glass (SG) phase is observed in the $R_2Mo_2O_7$ family.[8,10] The lack of long-range AF order and the modification of the usual AF-FM bicritical phase diagram[17] are ascribed to the highly frustrated pyrochlore lattice.

Since the itinerant $e(t_{2g})$ electrons mediate the double exchange (DE) interaction, the metallicity in this system is accompanied by ferromagnetic order. On the wider bandwidth side of the phase diagram reproduced in Fig. 1 (i.e., in case of R=Nd, Sm, and Eu) a coherent metallic state appears in an extended temperature range. We note, however, that an external field of ~14 T can fully polarize the Mo 4*d* spins also in the insulators.[18] It was also pointed out[14] that the SG-FM transition does not coincide with the MIT point, but the ferromagnetism can survive in the insulating phase beyond the MI phase boundary as it is the case for $Gd_2Mo_2O_7$. All these suggest that orbital degrees of freedom cannot be neglected in an appropriate microscopic model of pyrochlore-type molybdates.

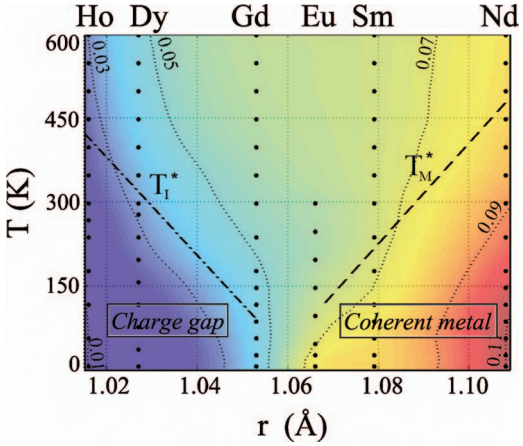

FIG. 1. (Color) Linear contour map of the spectral weight $N_{\mathrm{eff}}(\omega_{iso})$, where $\omega_{iso} \approx 0.5$ eV is the isosbestic point energy, on the temperature vs rare-earth ionic radius (r) plane. The surface is obtained by the interpolation of the experimental data indicated by black dots. Two crossover regions are indicated with T_M^* and T_I^*. Besides the color scaling, numerical values are also indicated on the contour lines.

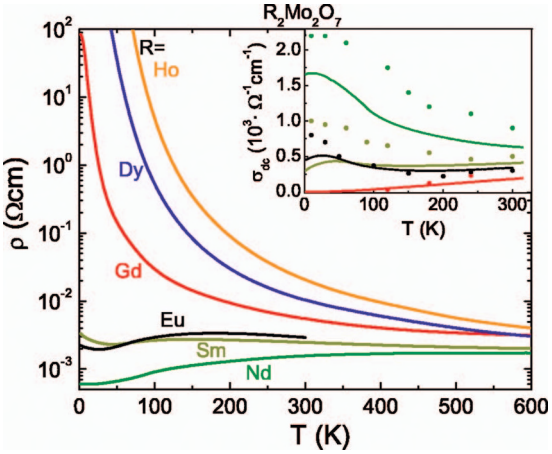

FIG. 2. (Color) Temperature dependence of the resistivity for six single crystals of $R_2Mo_2O_7$. The inset shows the comparison of σ_{dc} and $\sigma(\omega \rightarrow 0)$ below $T=300$ K for $R=$Gd, Eu, Sm, and Nd.

After describing the details of the experimental procedure in Sec. II, we first focus on the evolution of the ground state as a function of the rare-earth ionic radius (or alternatively the one-electron bandwidth) in Sec. III and then turn to the temperature-induced spectral changes in Sec. IV. A part of these results was published in a Letter.[14] However, this time we obtained the result of $Eu_2Mo_2O_7$ crystal, which locates in the immediate vicinity of the MI boundary at the metallic side, and therefore offers an even closer insight into the mechanism of the bandwidth-controlled MIT. Section V describes the systematics of the quasiparticle weight over the temperature-bandwidth phase diagram and the microscopic origin of the electron-phonon coupling observed for some of the infrared active phonon modes. Finally in Sec. VI, we discuss the effect of hole doping on the barely insulating $Gd_2Mo_2O_7$.

II. EXPERIMENTAL DETAILS

All of the $R_2Mo_2O_7$ samples ($R=$Nd, Sm, Eu, Gd, Dy, and Ho) investigated here were single crystals with a typical diameter of ~6 mm grown by a floating-zone method. In addition to these line compounds, we have studied the effect of hole doping on $Gd_2Mo_2O_7$ and $Nd_2Mo_2O_7$. These crystals were synthetized by the same technique, and the hole doping was realized by the partial substitution (δ) of the rare-earth R^{3+} ions with Ca^{2+}. The (111) crystallographic plane of the samples was cut and polished with alumina powder to the optical flatness.

Reflectivity spectra were measured in a photon-energy (E) range of 3 meV–6 eV at $T=10$–300 K and in a slightly limited range ($E \geqslant 80$ meV) at $T=10$–600 K.[19] For the proper Kramers-Kronig analysis the room-temperature measurements were extended up to 40 eV with use of synchrotron radiation at UV-SOR, Institute for Molecular Science. The resulting wide energy-range conductivity spectra of the two end materials ($R=$Nd and Ho) are shown in the inset of Fig. 2. [In our convention $\sigma(\omega)$ denotes the real part of the optical conductivity simply referred to as the optical conductivity.] The Mo $4d$ intraband excitations located below ~2 eV are clearly separated in case of $Nd_2Mo_2O_7$ from the higher energy O $2p \rightarrow$ Mo $4d$ charge-transfer excitations common for each compound. The conductivity minimum around 2 eV becomes less pronounced toward $Ho_2Mo_2O_7$, yet still reflects the separation of the two energy scales.

The temperature dependence of the dc resistivity for each compound was also measured on high-quality single crystals by the standard four-probe method. The extrapolated zero-frequency conductivity $\sigma(\omega \rightarrow 0)$ shows overall agreement with the dc resistivity data in each material as presented in the inset of Fig. 2 for $R=$Gd, Sm, Eu, and Nd.

III. EVOLUTION OF THE GROUND STATE

We have performed a systematic optical study on the evolution of the electronic structure upon the correlation-driven MIT by mapping an extended region of the bandwidth-temperature phase diagram. The effective one-electron bandwidth for the Mo $4d$ electrons is sensitive to the Mo-O-Mo bond angle and hence can be controlled by changing the rare-earth ionic radius r.[20] In fact, we found that even the discrete line compounds ($R_2Mo_2O_7$ with $R=$Nd, Sm, Eu, Gd, Dy, and Ho) offer an ideal laboratory to finely tune the electronic states in the vicinity of the MIT.

Figure 2 displays the temperature dependence of the six line compounds: $Ho_2Mo_2O_7$, $Dy_2Mo_2O_7$ and $Gd_2Mo_2O_7$ are insulators with decreasing charge gap in this order, while $Eu_2Mo_2O_7$ and $Sm_2Mo_2O_7$ are metals on the verge of the MIT and even $Nd_2Mo_2O_7$ with relatively larger bandwidth shows the characteristics of bad metals. All their resistivity is above the Ioffe-Regel limit (except for the low-temperature phase of $Nd_2Mo_2O_7$), $\rho_{\mathrm{IR}} \approx 0.5$ mΩ cm, the value anticipated with 1 conduction electron per Mo site. Irrespective of the ground-state nature, the $\rho(T)$ curves tend to converge toward high temperature without any sign of temperature-induced

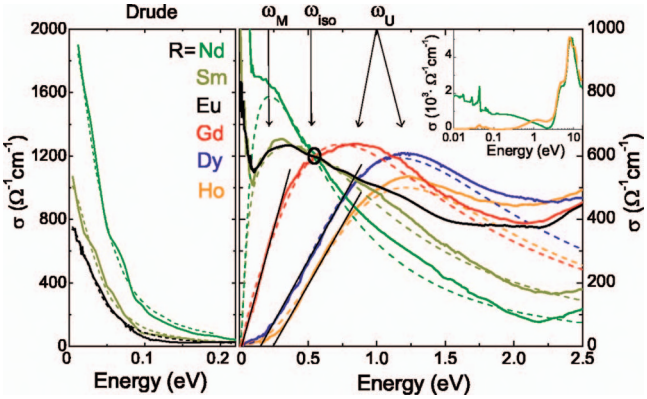

FIG. 3. (Color) Right panel: The $T=10$ K spectra of the $R_2Mo_2O_7$ family. The dashed lines are the fits based on the two oscillator terms of Eq. (1). The location of the related peaks and the isosbestic point are indicated by arrows. The extrapolation to estimate the gap energy is shown by black straight lines. The broader energy-range spectra for R=Ho and Nd are given in the inset. Left panel: The low-energy spectra of the three metals (R=Nd, Sm, and Eu) after the subtraction of the oscillator terms centered at ω_M and ω_U (see text). The dashed lines correspond the Drude fits.

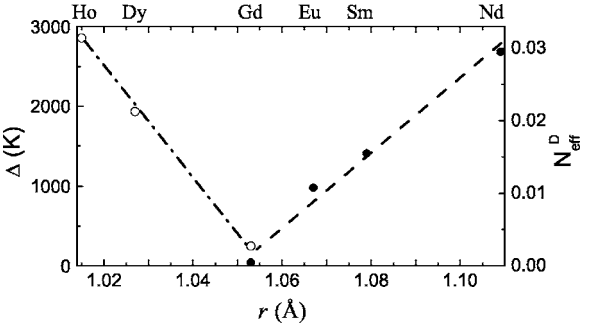

FIG. 4. R dependence of the charge gap Δ (closed circle) and the Drude weight N_{eff}^D (open circle) in the ground state.

MIT and the resistivity values range within a factor of two at $T=600$ K. In the metals the character of the charge transport undergoes a crossover like change toward high temperature: The resistivity of $Nd_2Mo_2O_7$ is saturated above 500 K and the behavior of $Sm_2Mo_2O_7$ becomes even semiconductorlike above 200 K. The smooth connectivity between the insulator and the metallic phase at finite temperatures as well as the extremely small mean free path in the metals suggest the ineffective screening of the Coulomb interaction in the whole temperature range and the hoppinglike incoherent conduction in the high-temperature state common to all the compounds.

For the study of the correlation-driven MI phenomenon, we focus on the intraband transitions of the Mo 4d electrons located below ~2 eV. The spectral shape of the four infrared active phonon modes (observed in the range of E =20–60 meV) will be discussed in Sec. V, while in the present analysis their contribution is subtracted from the raw data. The overview of the groundstate spectra is given in Fig. 3. The location of the broad maximum in the optical conductivity of the insulators around $\hbar\omega_U \approx 1$ eV corresponds to the effective on-site Coulomb interaction, U. The charge gap Δ can be clearly distinguished, and the gap values are determined by the linear extrapolation of the steeply increasing edge of the respective spectra as indicated in the figure. The observed Mott-Hubbard gap shows a systematic decrease with increasing r (see Fig. 4). $Ho_2Mo_2O_7$ and $Dy_2Mo_2O_7$ have a charge gap $\Delta \approx 250$ and 170 meV, respectively, comparable to the on-site Coulomb interaction, while $Gd_2Mo_2O_7$ is located at the barely insulating side of the phase diagram with almost zero gap; $\Delta \approx 20$ meV $\approx 0.02U$. For a larger ionic radius of the rare earth, the distinct change of the ground state is discerned as the system undergoes an insulator-to-metal transition at $r \gtrsim r(R=\text{Gd})$.

In going from $Gd_2Mo_2O_7$ to $Nd_2Mo_2O_7$, the recovery of the metallic character is manifested by the robust spectral weight transfer from the U peak simultaneously to a coherent (Drude) part and to an incoherent midinfrared (MIR) peak centered at $\hbar\omega_M \approx 0.2$ eV. This redistribution occurs through an equal-absorption (isosbestic) point located at $\hbar\omega_{iso}$ ≈ 0.5 eV. Such a spectral-weight transfer across the isosbestic point is a generic feature for the filling-controlled or thermally induced Mott transition.[4] (Although no temperature-induced metal-insulator transition is observed in the present materials, the isosbestic behavior also holds as a function of temperature, as will be shown in Sec. IV.) In the course of the bandwidth-controlled MIT, the existence of an isosbestic point can be attributed to the insignificant screening of U.

While in the spectrum of $Eu_2Mo_2O_7$ and $Sm_2Mo_2O_7$, the remains of the gapped feature are still discerned, the conductivity of $Nd_2Mo_2O_7$ is dominated by the Drude-like and the MIR peaks. Motivated by the presence of the equal-absorption point and the unambiguous separation of the different spectral features, we carried out a decomposition of the optical conductivity by the aforementioned three terms

$$\sigma(\omega) = \frac{D\gamma}{\gamma^2+\omega^2} + \sum_{i=M,U} \frac{A_i\omega^2\Gamma_i}{\omega^2\Gamma_i^2 + (\omega^2-\omega_i^2)^2}. \quad (1)$$

The first is the Drude component and the latter two asymmetric oscillators are for fitting of the charge gap excitation and the MIR peak. The latter one is possibly related to transitions from the quasiparticle peak to the upper Hubbard band (or from the lower Hubbard band to the quasiparticle peak). The applicability of Eq. (1) to the present systems is manifested by the fact that all the spectral features below ~2 eV can be well reproduced by only treating the weights (D, A_M, and A_U) and the scattering rate of the coherent part (γ) as fitting parameters. The characteristic energies, such as the center and the width (ω_i and Γ_i, respectively) of the oscillators, can be kept constant for these four compounds (R =Nd, Sm, Eu, and Gd), irrespective of temperature; $\hbar\omega_M$ =0.2 eV, Γ_M=0.8 eV, $\hbar\omega_U$=0.8 eV, and Γ_U=1.8 eV. Figure 3 shows the results of the fitting for the ground-state spectra. (Since the conductivity of $Eu_2Mo_2O_7$ and $Sm_2Mo_2O_7$ does not substantially differ below ~1 eV, the fitting for $Eu_2Mo_2O_7$ is not shown to keep the clarity of the figure.) After the subtraction of the oscillator terms, the low-energy part ($\hbar\omega \lesssim 0.2$ eV) shown in the left panel is well described by the Drude form with $\gamma \approx 35$ meV, independently of the rare earth. The spectrum of the insulators (R=Dy,Ho) lo-

cated far from the MIT boundary is well fitted by the single term of the charge gap excitations with slightly larger U corresponding to $\hbar\omega_U \approx 1.2$ eV.

As a paradigm for the Mott transition, the single-band Hubbard model with half filling has been intensively studied in frame of the dynamical mean-field theory (DMFT).[3,21–25] Within this approach, the conductivity spectrum of the low-temperature paramagnetic metallic phase displays three contributions similarly to those considered in Eq. (1).[3,21] Since in this model the upper and lower Hubbard bands are located symmetrically to the quasiparticle peak at $\pm U/2$, the MIR peak in $\sigma(\omega)$ appears at $U/2$ while the transitions between the two Hubbard bands are centered around U. The width of these two features is related to the bare bandwidth as $\Gamma_M = W/2$ and $\Gamma_U = W$. These predictions cannot be fully mapped to our experimental results since the MIR peak appears at considerably lower energy than expected, namely, at $\hbar\omega_M \approx U/4$. One possible reason for such a deviation is that in the DMFT calculations the **k** dependence is completely neglected (e.g., the model cannot account for the difference between direct and indirect gap), which could certainly affect both ω_U and ω_M. On the other hand, pyrochlore-type molybdates cannot be considered as a pure realization of the Hubbard model: (i) the bandwidth of the itinerant Mo $e(t_{2g})$ electrons is not related to direct hopping between neighboring Mo sites, but it is due to DE through oxygens; and (ii) the presence of localized Mo a_{1g} electrons close to the Fermi energy (and their mixing with the conduction band) is likely to shift the position of the quasiparticle band from the midpoint between the upper and the lower Hubbard bands. Nevertheless, on the basis of the semiempirical decomposition of the optical conductivity according to Eq. (1), we conclude that in these compounds both U and W are in the range of $\sim 1-2$ eV, and therefore, their ratio is in the order of unity that is the generally accepted criterion for the correlation-driven MIT in three dimensions.

As the measure of the spectral weight, the effective number of electrons N_{eff} contributing to the spectrum up to a certain energy, $\hbar\omega_c$, is defined as

$$N_{\text{eff}}(\omega_c) = \frac{2m_0}{\pi e^2 N} \int_0^{\omega_c} \sigma(\omega) d\omega, \tag{2}$$

where m_0 is the free electron mass and N is the number of Mo atoms per unit volume. After the decomposition of $\sigma(\omega)$ according to Eq. (1), the different weights are directly determined by the fits. The change in the character of the ground state is manifested in Fig. 4, where both the gap value (Δ) and the Drude weight (N_{eff}^D) are plotted against r. $\Delta(r_c - r)$ decreases linearly, where the critical value $r_c \approx 1.055$ Å is close to $Gd_2Mo_2O_7$. On the metallic side, the coherent peak is built up and N_{eff}^D increases in proportion to the distance from r_c. In accord with the increase of N_{eff} below the isosbestic point, the contribution of the U peak is reduced so that the total spectral weight of the Mo $4d$ band is roughly conserved among the materials ($N_{\text{eff}}^{\text{total}} = N_{\text{eff}}^D + N_{\text{eff}}^{\text{MIR}} + N_{\text{eff}}^U = 0.38 \pm 0.06$).

IV. CROSSOVER TOWARD THE HIGH-TEMPERATURE PHASE

Because of the proximity to the MIT point, thermal excitations radically change the electronic states in each compound. In the case of the metals, the low-energy spectral weight gradually decreases and, simultaneously, the role of the U peak becomes more stressful toward high temperature as shown in Fig. 5, where the reflectivity and conductivity spectra are simultaneously plotted over a broad range of temperature. The largest variation is observed for $Nd_2Mo_2O_7$, where the temperature dependence is saturated around $T_M^* = 500$ K after the complete loss of the quasiparticle weight and a remarkable reduction of the MIR conductivity. (The detailed analysis of the Drude term will be given in Sec. V.) The same tendency is found for $Sm_2Mo_2O_7$ and $Eu_2Mo_2O_7$ with $T_M^* \approx 240$ K and 150 K, respectively. As r approaches r_c, a high-temperature incoherent state common for these metals is realized at relatively lower temperatures. Since no thermally induced MIT occurs in any of these compounds, T_M^* can be viewed as a crossover temperature from the coherent metallic state to the high-temperature phase with fully incoherent low-energy transport.

At the insulating side, the effect of elevated temperature is reverse: the priority of the U peak is suppressed by the development of low-energy incoherent excitations (see Fig. 6). In the case of $Ho_2Mo_2O_7$, the in-gap states are filled and the charge gap closes at $T_I^* \approx 400$ K. Similarly to the metallic side, no sign of a thermally induced MIT is observed and, therefore, it is plausible to view T_I^* as the temperature scale of the crossover from the insulator to the high-temperature incoherent conductor. The crossover temperature is again lowered with increasing r toward r_c: $T_I^* \approx 300$ K and 120 K for $Dy_2Mo_2O_7$ and $Gd_2Mo_2O_7$, respectively.

Although the ground states are distinct on the two sides of r_c, the compounds tend to approach a universal incoherent conduction state above T_I^* and T_M^*. As we already noted, the ground-state spectra for R=Nd, Sm, Eu, and Gd form an isosbestic point at $\omega_{iso} = 0.5$ eV. The fact that the same remains valid as a function of temperature allows a systematic study of the total spectral-weight redistribution over the T-r plane around the MIT point by the analysis of $N_{\text{eff}}(\omega_{iso})$.

In light of the general relation between the effective number of electrons and the expectation value of the kinetic energy, $N_{\text{eff}}(\omega_{iso})$ accounts for the kinetic energy of electrons relating to both the Drude response and the MIR band (incoherent charge transport). Hence it captures the electronic-structural change relevant to the correlation-driven MIT.[4,26] Besides the temperature-induced suppression of the metallic character through the crossover region T_M^*, the resulting contour map in Fig. 1 shows how the in-gap states in the insulators become gradually involved with the conduction by the thermal agitation. Though the gap is closed above T_I^* as indicated in the figure, the low-energy conductivity remains fully incoherent. This incoherent state (IS) corresponds to the plateaulike green region of the phase diagram where the conduction is ascribed to hoppinglike electron transport.[14] The IS region is centered around r_c and becomes more extended with increasing temperature. The uniformity of the IS is re-

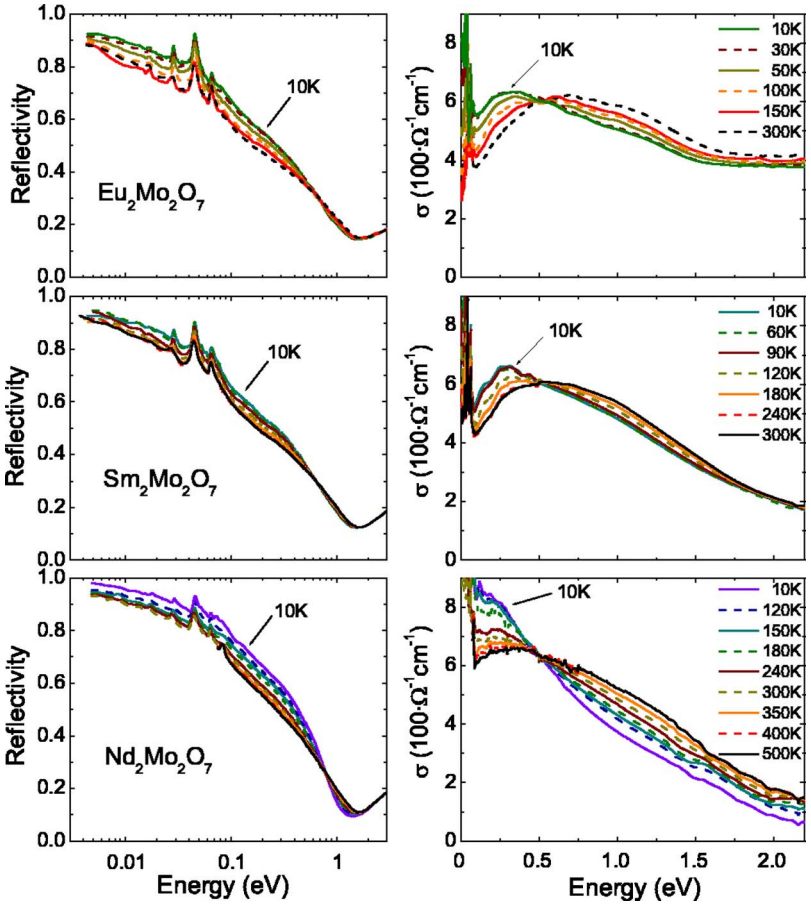

FIG. 5. (Color online) Reflectivity and conductivity spectra of the three metals R=Eu, Sm, and Nd at selected temperatures (left and right panel, respectively).

flected not only in $N_{\rm eff}(\omega_{iso})$, but the whole spectra in this region are essentially identical, irrespective of materials.

V. COHERENT CONDUCTION AND ELECTRON-PHONON INTERACTION

The temperature dependence of the low-energy ($\omega \lesssim 90$ meV) conductivity spectra for the metallic and insulating compounds is shown in the right and left panels of Fig. 6, respectively. As already mentioned, the conductivity spectra for both the metals and the insulators converge to a rather featureless incoherent spectrum at elevated temperatures by the gradual loss of the coherence and by the closing of the charge gap, respectively. In Sec. IV, the redistribution of the total spectral weight of Mo 4d electrons was discussed in terms of $N_{\rm eff}(\omega_{iso})$. Assuming that the scattering rate γ is roughly independent of the rare-earth radius r and also of the temperature (as can be checked in Fig. 7), we study the evolution of the quasiparticle weight in terms of $N_{\rm eff}(\omega_c)$ choosing ω_c=35 meV as the typical energy scale of γ. Furthermore, we subtract the residual optical weight common for the IS spectra $N_{\rm eff}(\gamma,{\rm IS})$ and evaluate the Drude weight over the r-T plane according to the relation that $N^{D}_{\rm eff}(\gamma;T,r) = N_{\rm eff}(\gamma;T,r) - N_{\rm eff}(\gamma;IS)$. The results are summarized in the top panel of Fig. 8(b). Although the Drude weight is considerably reduced on the ferromagnetic-to-paramagnetic transition, the coherent-incoherent crossover T^{*}_{M}, where the quasiparticle peak fades and merges into the frequency-independent incoherent background, occurs well above T_c. Since the scattering rate γ is enhanced only by $\sim$30% up to T^{*}_{M} the mass renormalization must play a major role in the loss of the coherence.

Now, we turn to the analysis of the IR active phonon modes whose contribution to the conductivity has been disregarded thus far. The unit cell of $R_2Mo_2O_7$ with the space group $Fd\bar{3}m$ consists of eight formula units. The factor group analysis yields the following optical-phonon modes:[28]

$$\Gamma^{\rm opt} = (A_{1g} + E_g + 4T_{2g}) + 7T_{1u}, \tag{3}$$

where the first six modes are Raman active and the seven T_{1u} are infrared active. In the far-infrared (FIR) region, we could clearly observe four phonon peaks at ω=17, 28, 44, and 63 meV.[27] The phonon resonances at ω_1=28 meV and ω_2=44 meV are assigned to bending modes in agreement with earlier studies on isostructural rare-earth titanates, stannates, zirconates, and hafnates.[28] The motion of the oxygen ions in the bending modes is perpendicular to the Mo-O-Mo bond, and therefore, the bond angle is effectively modulated as displayed in Fig. 8(a).

In the absence of strong electron-phonon interaction, the presence of mobile electrons generally results in the screening of the phonon resonances, especially in the region of the coherent electronic excitations. In contrast to this simple scenario, the two bending modes in $R_2Mo_2O_7$ pyrochlores become sharper when entering the metallic state. Moreover, the line shape of the two modes shows increasing asymmetry

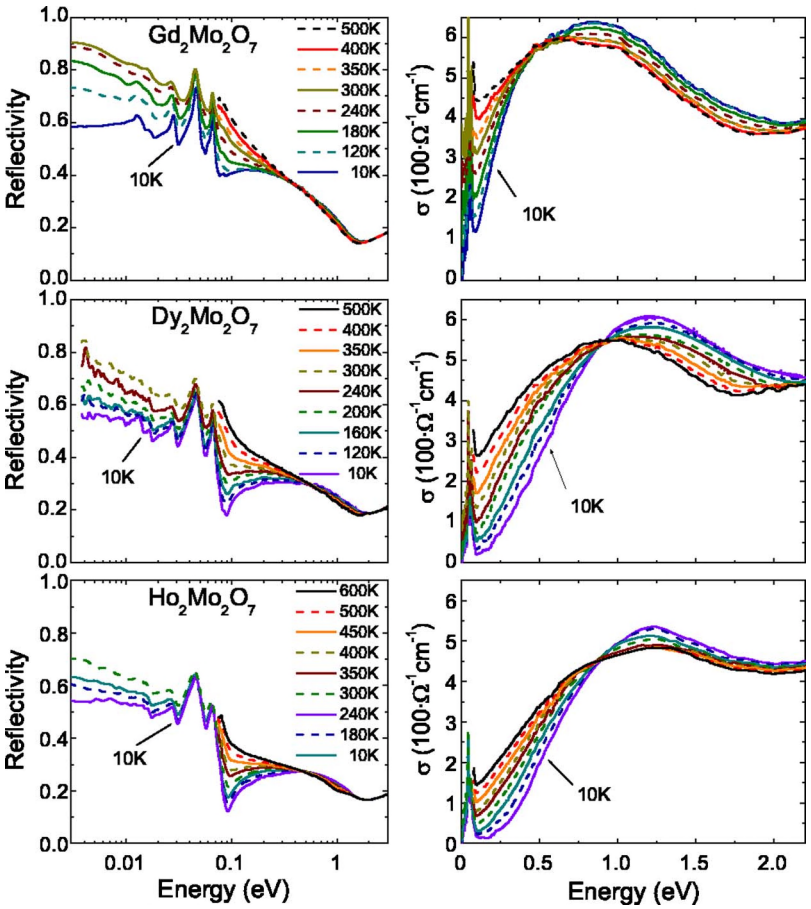

FIG. 6. (Color online) Reflectivity (left panel) and conductivity (right panel) spectra of the three insulators R=Gd, Dy, and Ho at selected temperatures.

when the metallic character is strengthened, indicating the role of electron-phonon coupling. We found that the contribution of theses phonons in the metallic compounds ($Nd_2Mo_2O_7$, $Sm_2Mo_2O_7$, and $Eu_2Mo_2O_7$) can be well fitted by the Fano resonance formula for the complex optical conductivity[29]

$$\tilde{\sigma}(\omega) = i\sigma_0(q-i)^2\left(i + \frac{\omega^2-\omega_i^2}{\gamma_i\omega}\right)^{-1}, \qquad (4)$$

where ω_i and γ_i are the resonant frequency and the linewidth of the vibrational state and q is the Fano asymmetry parameter. According to the original approach of Fano,[29] $1/q$ is roughly proportional to the interaction between the discrete resonance and the continuum, i.e., the electron-phonon interaction V_{e-ph} in our case. Both the resonance frequency and the linewidth are affected by V_{e-ph} and have the effective forms, $\omega_i=\omega_i^0+\Delta\omega_i$ and $\gamma_i=\gamma_i^0+\Delta\gamma_i$, where ω_i^0 and γ_i^0 describe the unperturbed phonon resonance. In the limit of $\gamma_i^0=0$, the determination of the electron-phonon coupling is straightforward since $\Delta\gamma_i=2\pi|V_{e-ph}|^2$. However, in the present case the separation of γ_i^0 and $\Delta\gamma_i$ is nontrivial. Therefore, we analyzed the line shape to determine the assymmetry parameter q for each compound below T=300 K. In the bottom panel of Fig. 8(b), $1/q$ for the bending modes ω_1 and ω_2 is plotted against the temperature. The result of the fitting is only shown for the ground-state spectra in Fig. 7. Fano derived the line shape given in Eq. (4) for a general transition probability. To apply the Fano model to the problem of the dielectric screening, Davis and Feldkamp[30] calculated the contribution of the discrete state coupled to a continuum to the dielectric function. The q values obtained by applying this procedure and determined by Eq. (4) coincide with each other within an accuracy of 5%. The fits for the imaginary part of the dielectric function in the metallic ground state are also shown in the insets of Fig. 7.

For the insulators, $1/q$ is small and positive as the phonons are weakly coupled to the electronic continuum of the U-peak tail. In $Gd_2Mo_2O_7$, the in-gap states are filled well below room temperature, resulting in a flat low-energy continuum around the phonon modes and consequently their asymmetry vanishes ~180 K. More remarkable is the case of the metals. The bending modes show large asymmetry corresponding to the phase shift as high as 50° in the ground state of $Nd_2Mo_2O_7$ and to slightly lower values for $Sm_2Mo_2O_7$ and $Eu_2Mo_2O_7$. The overall systematics is that the ferromagnetic to paramagnetic transition is accompanied by a sudden reduction of $1/q$ that is followed by a gradual decrease toward higher temperatures.

The effect of electron-phonon coupling on the line shape of Raman spectra is well described and used as a common tool to estimate the coupling strength.[31–33] However, there are very few examples where remarkable asymmetry is observed for infrared active phonon modes and analyzed in terms of the electron-phonon coupling. The contour maps in Fig. 9 give a comparison between the Drude weight and the phonon mode asymmetry $1/q$ below room temperature. The strong correlation between the two quantities is evident: the

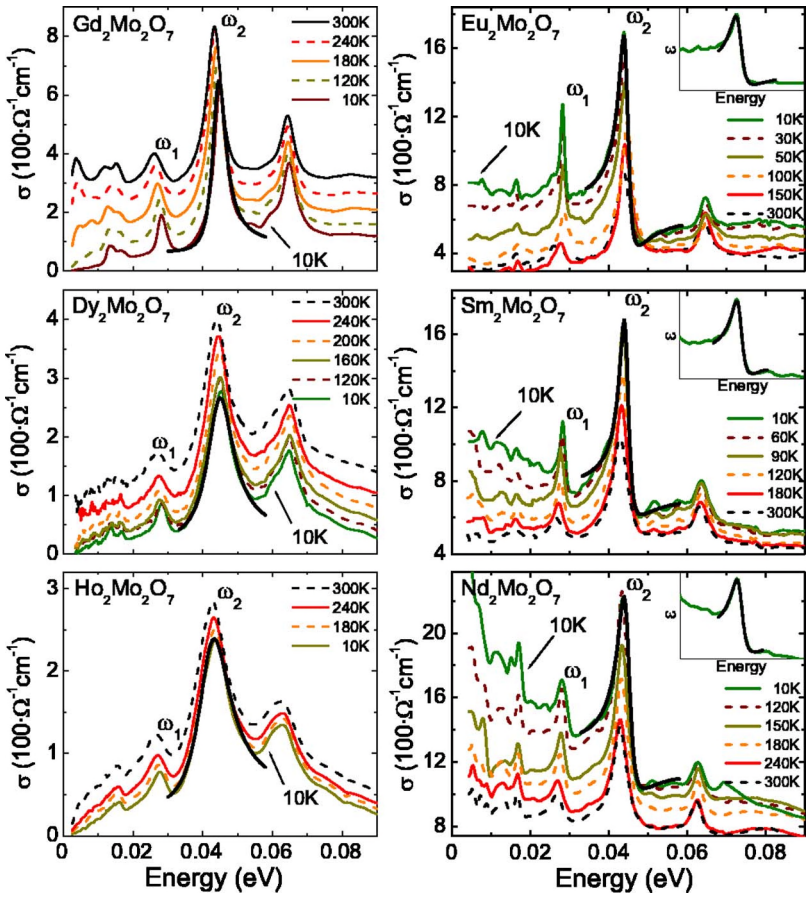

FIG. 7. (Color online) Low-energy conductivity spectra of the insulating and metallic compounds (left and right panel, respectively) at various temperatures below $T=300$ K. The peaks corresponding to the two bending modes are labeled by ω_1 and ω_2. The solid thick black lines represent the fitting of ω_2 phonon according to Eq. (4) in the ground state of each compound. In addition, for the metals the contribution of ω_2 resonance to the imaginary part of the dielectric function ϵ and the corresponding fit are also displayed in the insets.

asymmetry of the bending modes is observed as far as the coherence peak is preserved. The extremely large phonon phase shift (or asymmetry) is a consequence of the conduction channel for the Mo 4*d* electrons arising from the double exchange mechanism on the Mo-O-Mo bonds. In this term, the source of the electron-phonon interaction is that the bending modes directly modulate the bandwidth. Furthermore, the asymmetry of the phonons can be largely enhanced because their resonant frequency is in the range of the scattering rate of the coherent electrons ($\omega_1=28$ meV, $\omega_2=44$ meV, and $\gamma=35$ meV).

The bandwidth-controlled MIT in pyrochlore-type molybdates is also investigated by recent Raman scattering experiments.[13] As the MI phase boundary is approached from the metallic side, the intensity of the Raman active phonon modes coupled to the Mo 4*d* intraband excitations is suppressed and completely vanishes in the insulating phase. These Raman active phonons as an indicator of the MIT (A_{1g} at $\omega_{R1}\approx 61$ meV and the two-phonon excitation of the originally IR active resonance at $\omega_{R2}\approx 2\omega_1$) are also assigned to Mo-O-Mo bending modes. However, their energy is larger than either ω_1 or ω_2 and, consequently, they probe the electronic states further away from the Fermi level. It is particularly important in case of $Gd_2Mo_2O_7$ where the charge gap in the ground state is as small as $\Delta\approx 20$ meV. Since the A_{1g} Raman mode is located well above the gap, it cannot clearly distinguish between the insulating and metallic state unlike the bending modes observed in the far-infrared spectra.

VI. EFFECT OF HOLE DOPING ON METAL-INSULATOR TRANSITION

In the close vicinity of the Mott transition, the insulating state is usually unstable against the change of band filling.[26,34,35] We have investigated the effect of hole doping on the barely insulating $Gd_2Mo_2O_7$ and for comparison on the metallic $Nd_2Mo_2O_7$ for the nominal doping level (or equivalently the Ca^{2+} concentration relative to that of R^{3+}) $\delta=0$, 5, and 10 % and $\delta=0$, and 10%, respectively. All their ground-state ($T=10$ K) spectra are shown in Fig. 10. Generally speaking, the spectral weight of the Mo 4*d* band is enhanced for the both materials with increasing doping concentration. We found that the charge gap is closed in the 5% doped $Gd_2Mo_2O_7$ and its spectrum still crosses the isosbestic point at $\omega_{iso}=0.5$ eV (middle panel). For further doping, the isosbestic behavior does not hold any more and the conductivity is enhanced up to ~1 eV as observed in the both materials with $\delta=10\%$. The bottom panel focuses on the region of the quasiparticle excitations: in $Nd_2Mo_2O_7$ the Drude weight remains unchanged and in $Gd_2Mo_2O_7$, although the in-gap state are filled, no coherent conduction is established. The low-energy conductivity is fully incoherent and rather flat both for $\delta=5$ and 10 %. Correspondingly, the symmetric line shape of the two bending modes ω_1 and ω_2 is preserved. The whole conductivity spectra show very weak temperature dependence in the doped $Gd_2Mo_2O_7$ crystals as indicated in Fig. 11 where $\sigma(\equiv 1/\rho_{dc})$ obtained from resistivity measure-

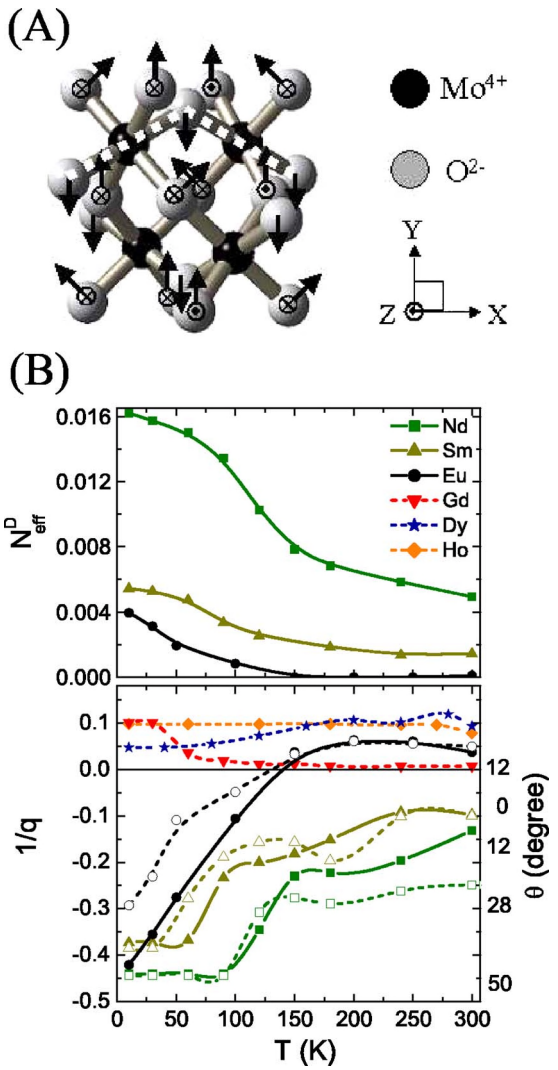

FIG. 8. (Color online) (a) Bending modes within the crystal structure. The arrows indicate the displacement of the O^{2-} ions, i.e., bending of the Mo-O-Mo bond. (b) Upper panel: Temperature dependence of the Drude weight in the metals (R=Nd, Sm, and Eu). Note that the actual value corresponds to the half of the Drude weight as the numerical integration in N_{eff}^{D} is done up to $\omega_c=\gamma$ (see the text for details). Lower panel: Temperature dependence of the inverse of the Fano asymmetry parameter $1/q$ obtained for the ω_2 bending mode (closed symbols) in each compound and for the ω_1 bending mode (open symbols) in the metals.

ment and $N_{\mathrm{eff}}(\omega_{iso})$ are simultaneously plotted. (The extrapolated zero-frequency optical conductivity $\sigma(\omega\rightarrow 0)$ shows overall agreement with the dc value for each compound.) The temperature dependence is somewhat weakened by hole doping also in the case of $Nd_2Mo_2O_7$. The above results imply that in addition to the hole doping effect the Ca^{2+} substitution on the R^{3+} site introduces considerable disorder to the system, which results in the strong scattering of the doped carriers. Therefore, they do not form a coherence peak, but their optical weight is mostly distributed over the MIR region.

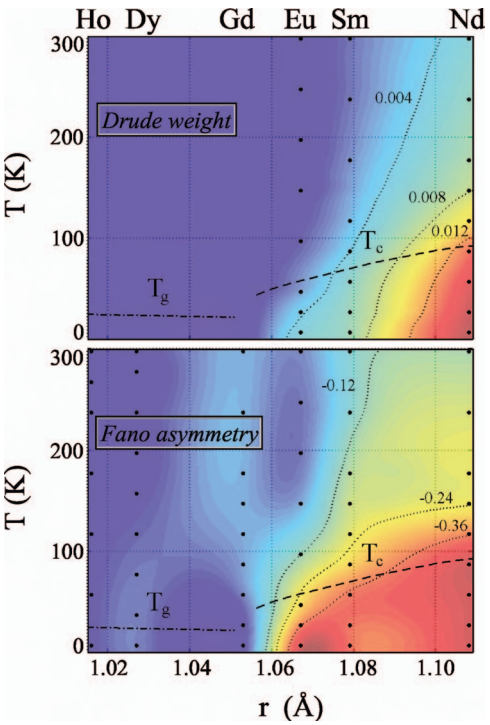

FIG. 9. (Color) Comparison of the quasiparticle weight and the Fano asymmetry on the temperature vs rare-earth ionic radius (r) plane. The contour plots were obtained by the interpolation of the experimental data shown in Fig. 7 indicated by black dots. Upper panel: Contour map of the Drude weight, N_{eff}^{D}. Lower panel: Contour map of inverse asymmetry parameter, $1/q$ for the ω_2 bending mode. The color scaling can be checked in both cases by the numerical values on the contour lines. The magnetic phase boundaries are also indicated by showing the FM (T_c) and SG transition (T_g) temperatures.

VII. CONCLUSIONS

We have studied the metal-insulator phenomena driven by the correlation of $4d$ electrons for pyrochlore $R_2Mo_2O_7$ single crytals by infrared spectroscopy. Both U and W estimated from the ground-state optical spectra are in the range of $\sim$1–2 eV. We identified the critical value (r_c) of the rare-earth ionic radius controlling the one-electron bandwidth W, where the T=0 K metal-insulator transition occurs. The transition point is located between $Gd_2Mo_2O_7$ and $Eu_2Mo_2O_7$ in the immediate vicinity of $Gd_2Mo_2O_7$. As this point is approached from the insulating and the metallic side, the charge gap and the Drude weight continuously vanish in proportion to $|r_c-r|$. In spite of the huge temperature-induced spectral weight transfer and the distinct change of the ground state, a finite-temperature discontinuous MIT is not observed in pyrochlore molybdates, neither in the present series nor in the chemically substituted compounds, $(R_x^1R_{1-x})_2Mo_2O_7$.[10,36] Instead, toward high temperature the states tend to form a common incoherent conduction phase through crossover temperatures T_M^* and T_I^*. On this basis we conclude that the metal-insulator transition is restricted to zero temperature. On the other hand, the very small charge gap realized in the ground state of $Gd_2Mo_2O_7$ ($\Delta/U\approx 0.02$) as well as the linear

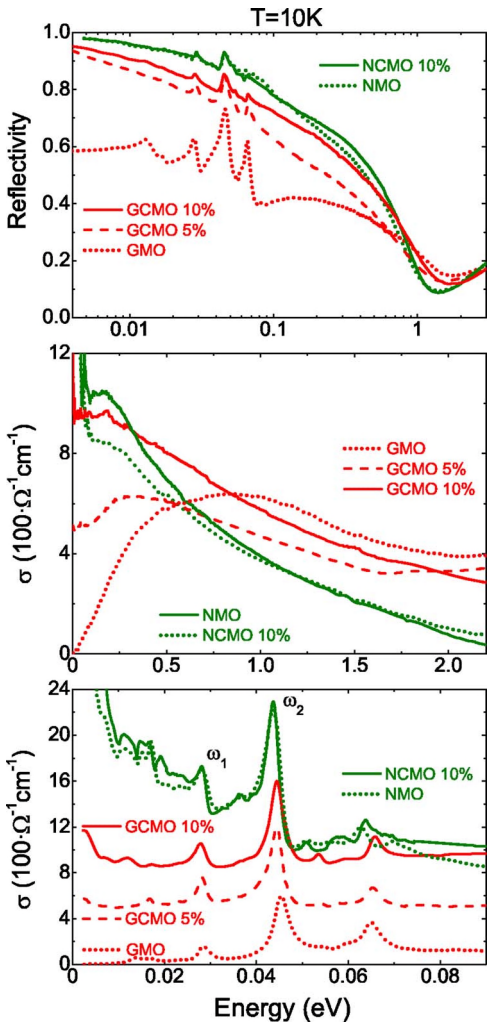

FIG. 10. (Color online) Reflectivity (top panel), broad-range conductivity (middle panel), and low-energy conductivity (bottom panel) spectra in the ground state of hole-doped $Gd_2Mo_2O_7$ (GCMO) and $Nd_2Mo_2O_7$ (NCMO) compounds for doping level of $\delta=0,5,10\,\%$ and $\delta=0,10\,\%$, respectively.

dependence of both $\Delta(r_c-r)$ and $N_{\mathrm{eff}}^{D}(r-r_c)$ implies that the MIT occurs without any discontinuity in the charge compressibility even at $T=0$ K. Therefore, the huge change in the electronic state over the T-r phase diagram is the consequence of the underlying zero-temperature quantum MI transition. On the other hand, general arguments suggest that a MIT is likely to become first-order before the predicted gap could completely vanish.[1] More qualitatively, recent DMFT calculations for the single-band Hubbard model[22,23,25] result in a crossover temperature $T_c \approx 0.02W$ below which the bandwidth-controlled MIT occurs (at the critical ratio $U/W \approx 1.2$) in a first-order manner and the transition is accompanied by a broad range of hysteresis. The results also indicate that the charge gap opens discontinuously. At $T>T_c$, the crossover from the metallic to the insulating state is narrow with a rapid suppression of the quasiparticle peak. The above estimate of the crossover temperature would correspond to $T_c \approx 200$ K for $R_2Mo_2O_7$. However, transport measurements reveal neither a temperature-nor pressure-induced MIT above ~ 1 K.

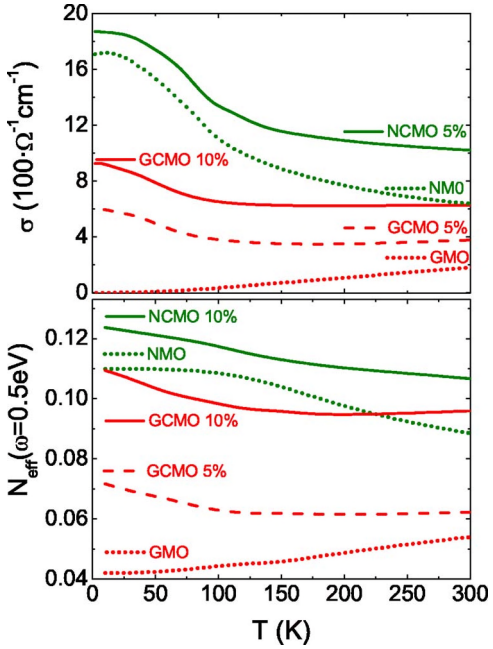

FIG. 11. (Color online) Temperature dependence of the dc conductivity (top panel) and the spectral weight below $\omega=0.5$ eV, $N_{\mathrm{eff}}(\omega=0.5\ \mathrm{eV})$ (bottom panel) hole doped $Gd_2Mo_2O_7$ (GCMO) and $Nd_2Mo_2O_7$ (NCMO) crystals.

The lack of first-order MIT in pyrochlore molybdates is supported by recent high-pressure experiments on $Gd_2Mo_2O_7$, which, in fact, evidenced the onset of a continuous MIT having Mott-Anderson character.[18] The possibility of zero-temperature Mott transition has recently been reconsidered by Imada.[37] He has pointed out when the MI transition temperature is sufficiently suppressed, i.e., close to or less than the Fermi temperature, the effect of quantum fluctuations becomes relevant. For $T_{\mathrm{MI}}=0$, instead of the usual quantum-critical point scenario, the existence of a marginally quantum-critical line is proposed since the insulating and metallic ground states must remain clearly distinguishable.

The unique nature of the phase diagram is ascribed to the interplay of several factors: (i) the near-critical ratio of the one-electron bandwidth and the effective Coulomb interaction, (ii) the competition of FM and AF exchange interaction for Mo $4d$ spins, (iii) the strong frustration of AF long-range order on pyrochlore lattice, and (iv) the coupling J_{f-d} between Mo $4d$ and R $4f$ spins. The first one governs the MI phenomenon. The second and third ones together with the incomplete quenching of the orbital degree of freedom within the $e_g(t_{2g})$ subspace are responsible for the lack of temperature-induced transition (replaced with crossover regions) and for the simultaneous suppression of the transition to zero temperature. Here we note that the paramagnetic phase above T_c is still metallic and the Drude weight vanishes well above T_c. This suggests that the magnetic ordering does not play a determinant role in the development of the coherent conduction but orbital degrees of freedom must also be considered. Finally, J_{f-d} introduces a built-in disorder potential for the Mo $4d$ electrons due to the glassy ground state of the R $4f$ spins and, therefore, results in the inevitable Anderson-like character of the MIT on the lowest energy

scale. The high sensitivity to the disorder around r_c is demonstrated by the filling control of the MI phenomenon in case of $Gd_2Mo_2O_7$. As a side effect of the hole doping, quenched disorder is introduced by the partial substitution of Gd^{3+} with Ca^{2+}. Consequently, no coherent metallic state can be established although the charge gap is closed by a tiny hole concentration $\delta < 5\%$. Besides the parameters mentioned above, electron-phonon interaction may also be relevant to the issue of the MIT. We observed unusually large Fano asymmetry for the two Mo-O-Mo bending modes in the metallic state. This is due to the electron-phonon coupling because these phonon modes directly modulate the effective one-electron bandwidth. However, it seems unlikely that electron-phonon scattering would play a major role in the electron localization itself as the crystal symmetry remains unchanged upon the MIT.[10]

ACKNOWLEDGMENTS

The authors are grateful to M. Imada and K. Taniguchi for enlightening discussions. This work was supported, in part, by a Grant-In-Aid for Scientific Research, MEXT of Japan. I.K. acknowledges support from JSPS and from ERATO Tokura Spin Superstructure Project, JST, and from the Bolyai János Foundation.

[1] N. F. Mott, Proc. Phys. Soc., London, Sect. A **49**, 72 (1949); **62**, 416 (1949); *Metal-Insulator Transitions* (Taylor & Francis, London, 1974).
[2] F. Kagawa, K. Miyagawa, and K. Kanoda, Nature (London) **436**, 534 (2005).
[3] A. Georges, G. Kotliar, W. Krauth, and M. J. Rozenberg, Rev. Mod. Phys. **68**, 13 (1996).
[4] M. Imada, A. Fujimori, and Y. Tokura, Rev. Mod. Phys. **70**, 1039 (1998).
[5] Y. Taguchi, Y. Oohara, H. Yoshizawa, N. Nagaosa, and Y. Tokura, Science **291**, 2573 (2001).
[6] A. P. Mackenzie and Y. Maeno, Rev. Mod. Phys. **75**, 657 (2003).
[7] I. Kézsmárki, S. Onoda, Y. Taguchi, T. Ogasawara, M. Matsubara, S. Iguchi, N. Hanasaki, N. Nagaosa, and Y. Tokura, Phys. Rev. B **72**, 094427 (2005).
[8] N. Ali, M. P. Hill, S. Labroo, and J. E. Greedan, J. Solid State Chem. **83**, 178 (1989).
[9] N. Cao, T. Timusk, N. P. Raju, J. E. Greedan, and P. Gougeon, J. Phys.: Condens. Matter **7**, 2489 (1995).
[10] T. Katsufuji, H. Y. Hwang, and S.-W. Cheong, Phys. Rev. Lett. **84**, 1998 (2000).
[11] Y. Taguchi, K. Ohgushi, and Y. Tokura, Phys. Rev. B **65**, 115102(R) (2002).
[12] M. W. Kim, Y. S. Lee, T. W. Noh, Jaenjun Yu, and Y. Moritomo, Phys. Rev. Lett. **92**, 027202 (2004).
[13] K. Taniguchi, T. Katsufuji, S. Iguchi, Y. Taguchi, H. Takagi, and Y. Tokura, Phys. Rev. B **70**, 100401(R) (2004).
[14] I. Kézsmárki, N. Hanasaki, D. Hashimoto, S. Iguchi, Y. Taguchi, S. Miyasaka, and Y. Tokura, Phys. Rev. Lett. **93**, 266401 (2004).
[15] J. S. Kang, Y. Moritomo, Sh. Xu, C. G. Olson, J. H. Park, S. K. Kwon, and B. I. Min, Phys. Rev. B **65**, 224422(R) (2002).
[16] I. V. Solovyev, Phys. Rev. B **67**, 174406 (2003).
[17] Y. Tokura, Psychol. Today **56**, 50 (2003), and references therein.
[18] N. Hanasaki, M. Kinuhara, I. Kézsmárki, S. Iguchi, S. Miyasaka, N. Takeshita, C. Terakura, H. Takagi, and Y. Tokura, Phys. Rev. Lett. (to be published).
[19] For some of these materials the optical conductivity have been previously measured below $T=300$ K by Refs. 9, 11, and 12.
[20] Y. Moritomo, S. Xu, A. Machida, T. Katsufuji, E. Nishibori, M. Takata, M. Sakata, and S. W. Cheong, Phys. Rev. B **63**, 144425(R) (2001).
[21] M. J. Rozenberg, G. Kotliar, and H. Kajueter, Phys. Rev. B **54**, 8452 (1996).
[22] J. Schlipf, M. Jarrell, P. G. J. van Dongen, N. Blümer, S. Kehrein, Th. Pruschke, and D. Vollhardt, Phys. Rev. Lett. **82**, 4890 (1999).
[23] R. Bulla, Phys. Rev. Lett. **83**, 136 (1999).
[24] M. J. Rozenberg, R. Chitra, and G. Kotliar, Phys. Rev. Lett. **83**, 3498 (1999).
[25] R. Bulla, T. A. Costi, and D. Vollhardt, Phys. Rev. B **64**, 045103 (2001).
[26] T. Katsufuji, Y. Okimoto, and Y. Tokura, Phys. Rev. Lett. **75**, 3497 (1995).
[27] These phonon energies are determined in the ground state of $Nd_2Mo_2O_7$. They slightly vary depending on the rare earth and harden toward low temperatures.
[28] M. T. Vandenborre, E. Husson, and H. Brusset, Spectrochim. Acta, Part A **37A**, 113 (1981); M. T. Vandenborre, E. Husson, J. P. Chatry, and D. Michel, J. Raman Spectrosc. **14**, 63 (1983).
[29] U. Fano, Phys. Rev. **124**, 1866 (1961).
[30] L. C. Davis and L. A. Feldkamp, Phys. Rev. B **15**, 2961 (1977).
[31] S. Naler, M. Rübhausen, S. Yoon, S. L. Cooper, K. H. Kim, and S. W. Cheong, Phys. Rev. B **65**, 092401 (2002); H. Rho, S. L. Cooper, S. Nakatsuji, H. Fukazawa, and Y. Maeno, *ibid.* **68**, 100404(R) (2003).
[32] D. L. Mills, A. A. Maradudin, and E. Burstein, Ann. Phys. (N.Y.) **56**, 504 (1970).
[33] T. Katsufuji and Y. Tokura, Phys. Rev. B **50**, 2704 (1994).
[34] Y. Okimoto, T. Katsufuji, Y. Okada, T. Arima, and Y. Tokura, Phys. Rev. B **51**, 9581 (1995).
[35] S. Onoda and M. Imada, J. Phys. Soc. Jpn. **70**, 3398 (2001).
[36] S. Iikubo, S. Yoshii, T. Kageyama, K. Oda, Y. Kondo, K. Murata, and M. Sato, J. Phys. Soc. Jpn. **70**, 212 (2000).
[37] M. Imada, Phys. Rev. B **72**, 075113 (2005).